universe

MDPI

Article

Thermal Profile of Accretion Disk Around Black Hole in 4D Einstein–Gauss–Bonnet Gravity

Odilbek Kholmuminov [1], Bakhtiyor Narzilloev [2,3,4,5,6] and Bobomurat Ahmedov [1,2,3,*]

[1] Institute of Fundamental and Applied Research, National Research University TIIAME, Kori Niyoziy 39, Tashkent 100000, Uzbekistan; xolmominovodilbek308@gmail.com
[2] Department of Physics, New Uzbekistan University, Movarounnahr Str. 1, Tashkent 100000, Uzbekistan; baxtiyor@astrin.uz
[3] Ulugh Beg Astronomical Institute, Astronomy Str. 33, Tashkent 100052, Uzbekistan
[4] Department of Mathematics, University of Tashkent for Applied Sciences, Str. Gavhar 1, Tashkent 100149, Uzbekistan
[5] Shahrisabz State Pedagogical Institute, Shahrisabz Str. 10, Shahrisabz 181301, Uzbekistan
[6] Institute of Engineering Physics, Samarkand State University, University Avenue 15, Samarkand 140104, Uzbekistan
* Correspondence: ahmedov@astrin.uz

Abstract: In this study, we investigate the properties of a thin accretion disk around a static spherically symmetric black hole in 4D Einstein–Gauss–Bonnet gravity, with an additional coupling constant, α, appearing in the spacetime metric. Using the Novikov–Thorne accretion disk model, we examine the thermal properties of the disk, finding that increasing α reduces the energy, angular momentum, and effective potential of a test particle orbiting the black hole. We demonstrate that α can mimic the spin of a Kerr black hole in general relativity up to $a \simeq 0.23$ M for the maximum value of α. Our analysis of the thermal radiation flux shows that larger α values increase the flux and shift its maximum towards the central black hole, while far from the black hole, the solution recovers the Schwarzschild limit. The impact of α on the radiative efficiency of the disk is weak but can slightly alter it. Assuming black-body radiation, we observe that the disk's temperature peaks near its inner edge and is higher for larger α values. Lastly, the electromagnetic spectra reveal that the disk's luminosity is lower in Einstein–Gauss–Bonnet gravity compared to general relativity, with the peak luminosity shifting toward higher frequencies, corresponding to the soft X-ray band as α increases.

Keywords: black hole; accretion disk; general relativity; Einstein–Gauss–Bonnet gravity

Academic Editor: Alexandre Marcowith

Received: 31 October 2024
Revised: 8 January 2025
Accepted: 24 January 2025
Published: 26 January 2025

Citation: Kholmuminov, O.; Narzilloev, B.; Ahmedov, B. Thermal Profile of Accretion Disk Around Black Hole in 4D Einstein–Gauss–Bonnet Gravity. *Universe* **2025**, *11*, 38. https://doi.org/10.3390/universe11020038

1. Introduction

Several alternative theories have emerged in efforts to address fundamental issues that General Relativity cannot fully resolve, such as the development of quantum gravity and the singularity problem. Most of such theories introduce higher-order curvature corrections to the Einstein–Hilbert action, with the Einstein–Gauss–Bonnet theory standing out as one of the most promising approaches. This theory involves quadratic curvature terms and is extended to higher orders by the Lovelock generalization. In four-dimensional spacetime, meaningful modifications to the equations of motion in the Einstein–Gauss–Bonnet framework arise only when the Gauss–Bonnet term is linked to a matter field, such as a dilaton. Different phenomena within these Einstein–dilaton–Gauss–Bonnet frameworks have been studied in works like [1–10]. It has been suggested [11] that a non-trivial Einstein–Gauss–Bonnet theory of gravity could exist without any extra fields

coupled to curvature. This claim posits that a generally covariant modified theory of gravity can exist in four-dimensional spacetime ($D = 4$) where only the massless graviton propagates, bypassing Lovelock's theorem [11] through a specific limit where $D \to 4$ from a higher-dimensional context. In this specific limit, the Gauss–Bonnet invariant contributes significantly to gravitational dynamics while maintaining the graviton degrees of freedom and avoiding Ostrogradsky instability. However, subsequent studies have shown that this regularization scheme fails for arbitrary metrics, implying that the regularization cannot be considered a well-defined theory [12–15].

A consistent formulation of the 4D theory was proposed in [16], where the Hamiltonian theory was developed using the ADM decomposition. This approach introduces a breaking of diffeomorphism invariance in a way that remains observationally viable. The theory is well defined, lacking any additional scalar degrees of freedom, thereby avoiding the issue of infinite coupling. Importantly, the black hole solution introduced in the original work [11] also meets the field equations of the rigorously formulated theory presented in [16]. Additionally, a later study by Aoki, Gorji, and Mukohyama [17], which focused on a cosmological solution, demonstrated that the dispersion relations for gravitational perturbations are altered in the ultraviolet regime. Consequently, it is anticipated that in the infrared regime, particularly for sufficiently massive black holes, the gravitational spectra can be accurately characterized by the original simplified model from [11], provided that the higher-dimensional perturbation equations permit dimensional regularization. It is also important to highlight that we have thoroughly explored different black hole solutions in prior studies, employing a variety of approaches [18–26].

Building on this foundation, our research has investigated diverse radiative, optical, and energetic characteristics of black holes in prior research papers. From an astrophysical perspective, analyzing observational data of thin accretion disks around black holes alongside predicted thermal spectra provides a powerful means of exploring gravity in its strong-field regime. This work utilizes this approach to examine the properties of the innermost stable circular orbits in the spacetime of a non-rotating black hole within 4D Einstein–Gauss–Bonnet gravity. Furthermore, we investigate the fundamental features of the geometrically thin and optically thick Novikov–Thorne accretion disk model surrounding such black holes. Specifically, we examine temperature profiles and spectral energy profiles of a Novikov–Thorne thin disk and contrast these findings with those derived from standard black holes within the framework of general relativity (GR). This comparative analysis aims to discern potential deviations or unique signatures that may arise when considering black holes in the context of modified gravity theories.

The structure of the work is as follows: Section 2 delves into the characteristics of spacetime surrounding a static black hole in 4D EGB gravity. Section 3 introduces the Novikov–Thorne model, focusing on an accretion disk encircling a black hole. This section elaborates on the accretion disk's properties, considering its geometric thinness and optical thickness. Section 4 addresses various aspects including the radiant energy flux across the accretion disk, the disk's radiative efficiency, temperature distribution, and the spectrum of thermal radiation emitted from its surface. Finally, Section 5 offers a synthesis of the key findings presented in the work. Throughout the text, we employ geometrized units where G = c = 1, employ Greek indices taking integer values from 0 to 3, and adopt a signature of spacetime where the time component is negative (−,+,+,+).

2. The New 4D EGB Theory and Black Hole Metric

In 4D spacetime, GR is governed by the Einstein–Hilbert action that reads

$$S_{EH} = \int d^D x \sqrt{-g} \left[\frac{M_P^2}{2} R \right]. \tag{1}$$

Here, $D = 4$ and the reduced Planck mass M_P characterizes the strength of gravitational coupling. As per Lovelock's theorem [27–29], GR is the sole theory of gravity in four dimensions, provided the following assumptions hold: (a) diffeomorphism invariance, (b) metricity, and (c) second-order equations of motion. Dimensions higher than four satisfying these action criteria are as follows:

$$S_{GB} = \int d^D x \sqrt{-g} \alpha G, \tag{2}$$

with α, the GB coupling constant, being dimensionless and G being the GB invariant, $G = R^{\mu\nu}_{\rho\sigma} R^{\rho\sigma}_{\mu} \nu - 4R^{\mu}_{\nu} R^{\nu}_{\mu} + R^2 = 6R^{\mu\nu}_{[\mu\nu} R^{\rho\sigma}_{\rho\sigma]}$. The approach proposed in [11] involves rescaling the coupling constant

$$\alpha \to \alpha/(D-4) \tag{3}$$

associated with the Gauss–Bonnet term, followed by taking the limit $D \to 4$. This results in a solution for the static and spherically symmetric case in an arbitrary number of dimensions $D \geq 5$:

$$ds^2 = -f(r)dt^2 + f^{-1}(r)dr^2 + r^2 d\Omega^2_{D-2}. \tag{4}$$

This solution, which was previously discovered in Ref. [30] (and also discussed in [31–33]), is extended to $D = 4$ solutions through the rescaling outlined in [11], followed by taking the limit $D \to 4$:

$$f(r) = 1 + \frac{r^2}{\alpha} \left[1 - \left(1 + \frac{4\alpha M}{r^3} \right)^{1/2} \right] \tag{5}$$

By utilizing L'Hopital's rule, one finds that $\lim_{\alpha \to 0} f(r) = 1 - \frac{2M}{r}$, showing that in this limit the line-element (4) reduces to the Schwarzschild line-element. The external black hole solution is valid for coupling constant values of α within the range

$$-16M^2 \leq \alpha \leq 2M^2. \tag{6}$$

Figure 1 illustrates how the metric function varies with changes in the radial coordinate for different values of α. It can be easily proven that as the radial coordinate approaches infinity, the function converges to one. This convergence effectively brings the spacetime metric to the form of Minkowski spacetime expressed in Boyer–Lindquist coordinates. Additionally, closer to the central compact gravitating object, the effect of the Gauss–Bonnet term becomes considerable. This influence is expected to impact photon radiation and other characteristics of the disk surrounding a black hole. Consequently, the primary objective of the study is to explore these effects.

The radius of the event horizon can be determined by locating the point where the function f(r) equals zero. The condition $f(r_h) = 0$ gives $\frac{r_h}{M} = 1 \pm \sqrt{1 - \frac{\alpha}{2M^2}}$. With $+$, this gives the black curve in Figure 2. It is observable that decreasing α leads to a larger event horizon, thereby strengthening the gravitational field. This phenomenon occurs since a more intense gravitational field allows a black hole to trap particles, including photons,

emitted from farther away, consequently expanding the size of the event horizon.

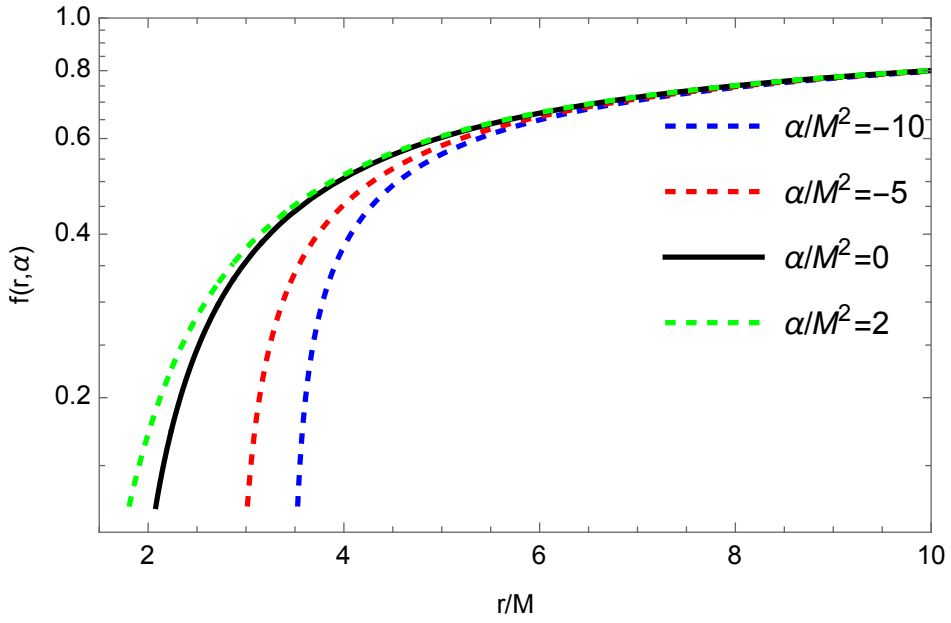

Figure 1. Radial variation of the metric function for the chosen values of the Gauss–Bonnet coupling constant.

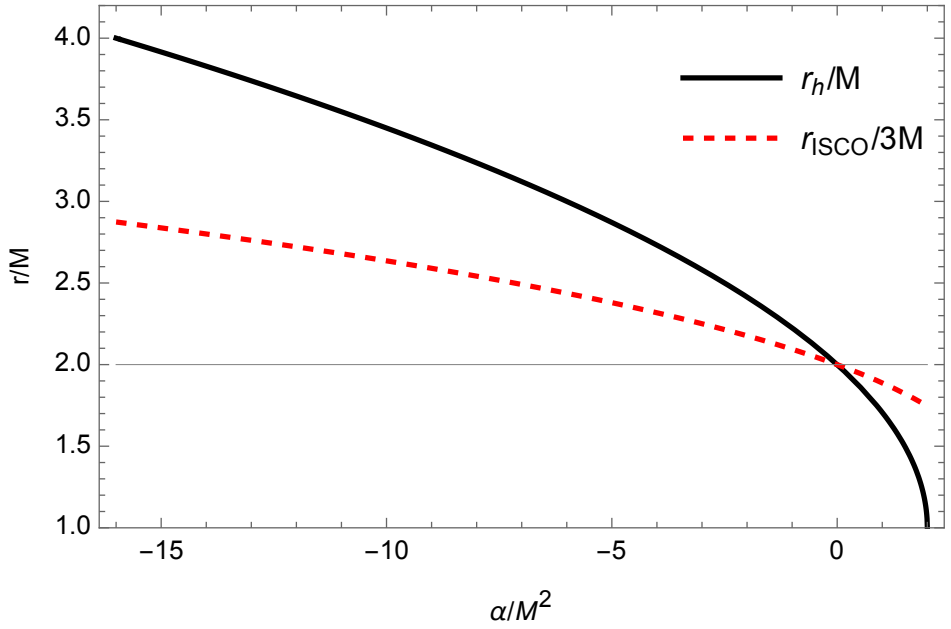

Figure 2. Variation of the event horizon radius (represented by the black solid line) and the re-scaled Innermost Stable Circular Orbit (ISCO) radius (red dashed line) on the Gauss–Bonnet coupling constant (see also [34]).

3. Thin Accretion Disk Model of Novikov and Thorne

In our analysis, we adopt the Novikov–Thorne model, which assumes that the accretion disk surrounding the central black hole is geometrically thin but optically thick [35]. This thinness primarily applies to the vertical dimension of the disk, which is consistently dwarfed by its significantly longer horizontal extension. Consequently, the height h of the disk, representing its maximum half thickness vertically, remains markedly less than the radius r of the disk horizontally, that is, $h \ll r$. In the context of hydrodynamic equilibrium

within the thin disk, both the gradient of pressure and the vertical gradient of entropy in the accreting material are deemed insignificant. This equilibrium state ensures that the disk avoids the buildup of heat produced by stresses with dynamical friction, as effective cooling through thermal radiation occurs across its entire surface. As a result, the thin vertical dimension of the disk remains stable. Positioned at the marginally stable orbit around central black hole, the inner edge of the thin disk hosts accreting plasma engaged in classical Keplerian motion, while higher orbits exhibit similar behavior.

In steady-state models of accretion disks, the rate of mass accretion $\dot{M}_0$ stays consistent over time. The properties of the orbiting plasma are typically described through averaged physical quantities over a characteristic time scale, denoted as Δt, covering the total orbit period across the azimuthal angle $\Delta\phi = 2\pi$ and vertical height h [35–37]. The effective potential governing the motion of a massive particle moving around a compact object can be expressed as per references [35,37,38] as follows:

$$V_{eff} = -1 + \frac{E^2 g_{\phi\phi} + 2EL g_{t\phi} + L^2 g_{tt}}{g_{t\phi}^2 - g_{tt} g_{\phi\phi}} = 1 + \frac{r^2 + 16(-1 - \frac{r^2(1-\sqrt{1+\frac{4\alpha}{r^3}})}{\alpha})}{r^2(1 + \frac{r^2(1-\sqrt{1+\frac{4\alpha}{r^3}})}{\alpha})}, \tag{7}$$

for the unit mass of a black hole. In the expression above, L and E represent the specific angular momentum and specific energy of a massive particle, respectively. Assuming that the trajectory of particles is circular, these conserved quantities can be formulated in terms of the metric tensor as follows:

$$E = -\frac{g_{tt} + \Omega g_{t\phi}}{\sqrt{-g_{tt} - 2\Omega g_{t\phi} - \Omega^2 g_{\phi\phi}}} = \frac{\alpha + r^2(1 - \sqrt{1 + \frac{4\alpha}{r^3}})}{\alpha\sqrt{\frac{r^3+4\alpha-3r^2\sqrt{1+\frac{4\alpha}{r^3}}}{r^3+4\alpha}}}, \tag{8}$$

and

$$L = \frac{\Omega g_{\phi\phi} + g_{t\phi}}{\sqrt{-g_{tt} - 2\Omega g_{t\phi} - \Omega^2 g_{\phi\phi}}} = \frac{r^2\sqrt{\frac{r^3(1-\sqrt{1+\frac{4\alpha}{r^3}})+\alpha(4-\sqrt{1+\frac{4\alpha}{r^3}})}{\alpha(r^3+4\alpha)}}}{\sqrt{\frac{r^3+4\alpha-3r^2\sqrt{1+\frac{4\alpha}{r^3}}}{r^3+4\alpha}}}. \tag{9}$$

Here, the angular velocity is

$$\Omega = \frac{d\phi}{dt} = \frac{-g_{t\phi,r} \pm \sqrt{(-g_{t\phi,r})^2 - (g_{\phi\phi,r})(g_{tt,r})}}{g_{\phi\phi,r}} = \sqrt{\frac{r^3(1 - \sqrt{1 + \frac{4\alpha}{r^3}}) + \alpha(4 - \sqrt{1 + \frac{4\alpha}{r^3}})}{\alpha(r^3 + 4\alpha)}}. \tag{10}$$

Radial profiles of the above quantities, namely, Ω, E, L, V_{eff}, are shown in Figure 3. From the top-left panel of Figure 3, it can be seen that for non-negative values of α the behavior of angular velocity Ω is similar to that of a Schwarzschild black hole, being slightly lower in value, while for negative α, its value starts rising exponentially near the central black hole. The effect of α reduces quickly with the increase in distance from the black hole. The radial dependence of the specific energy of a test particle making a circular revolution around a black hole is given in the top-right panel of Figure 3. One can see that the effect of α becomes noticeable only in the distances lower than the ISCO of test particles while in the outer orbits, its value does not differ from its rest energy at infinity considerably. One can also see that with the increase in α, the orbits where circular motion is allowed shift toward the central black hole. In the bottom-left panel of Figure 3, the dependence of the angular momentum of a test particle from the radial coordinate is shown for the circular motion of a particle. It can be seen that with the decrease in α, the angular momentum needed for

the test particle to stay at the same circular orbit increases. In the bottom-right panel of Figure 3, the radial profile of the effective potential of a test particle for the fixed values of its specific energy and angular momentum is shown. One can see that for negative values of α, the behavior of the lines is similar to that of a Schwarzschild black hole ($\alpha = 0$) and always positive. In contrast, for positive α, there is a region of spacetime where effective potential becomes negative, thereby limiting the possible region of spacetime where the motion of massive test particles is now allowed for the chosen values of the energy and angular momentum of a test particle. It is worth reminding here that in this case, we are not talking about the circular motion of a test particle as in the previous cases where we required the following condition to be satisfied: $V_{eff}(r) = V'_{eff}(r) = 0$.

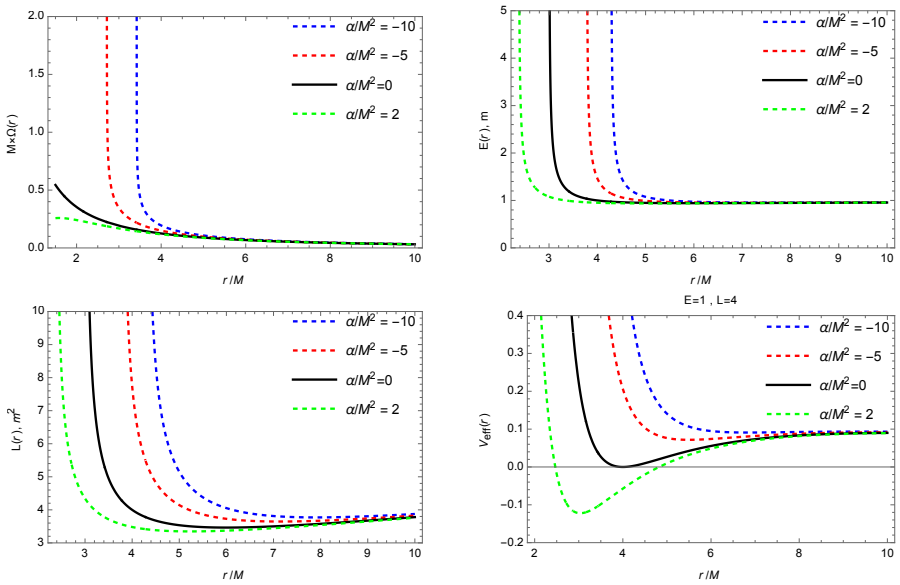

Figure 3. Radial dependence of Ω, E, L, V_{eff} for selected values of Gauss–Bonnet coupling constant.

In the selected model, the inner edge of the accretion disk encircling the compact object aligns with the ISCO of test particles making circular motion around the black hole at the core. By establishing three conditions based on the massive particle's effective potential,

$$V_{eff}(r) = 0, \qquad V'_{eff}(r) = 0, \qquad V''_{eff}(r) = 0, \tag{11}$$

we can determine the ISCO radius as a function of an additional spacetime parameter, as illustrated in Figure 2 by the red dashed line. From the figure, it is evident that a decrease in the values of the Gauss–Bonnet coupling constant results in a larger ISCO radius, akin to the event horizon radius, for reasons previously elucidated. It is well known that a decrease in the spin of a Kerr black hole also increases the ISCO radius of particles orbiting around rotating the black hole. Thus, it might be interesting to test how well the Gauss–Bonnet coupling constant α can mimic the spin a of the Kerr black hole for matching the ISCO radius of massive particles. This degeneracy is illustrated in Figure 4. The figure clearly illustrates that α can effectively replicate the impact of the rotation parameter on the ISCO radius of the retrograde motion of particles at the innermost part of the disk. It appears that negative values of α can mimic the retrograde spin up to $a/M \sim -0.87$, as indicated in the figure. For prograde motion, positive α can mimic the spin up to $a/M \sim 0.23$.

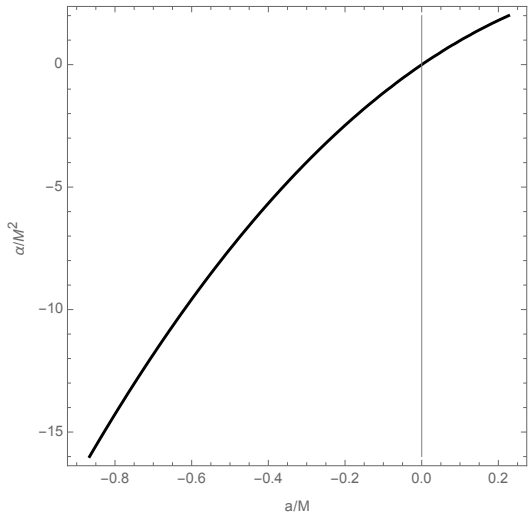

Figure 4. The degeneracy between the Gauss–Bonnet coupling constant α and the black hole rotation parameter a as reflected in the ISCO location.

4. Radiative Characteristics of the Accretion Disk Surrounding a Central Black Hole

Concerning the characteristics of the accretion disk, our primary focus is to investigate the radiant energy flux throughout the disk, along with its radiative efficiency, temperature distribution, and the spectrum of radiation coming from the disk because of the thermal radiation.

The expression for the flux of electromagnetic radiation coming from the accretion disk is provided as follows [35,37]:

$$F(r) = -\frac{\dot{M}_0 c^2}{4\pi M^2} \frac{\Omega_{,r}}{\sqrt{-g}(E-\Omega L)^2} \int_{r_{ISCO}}^{r} (E-\Omega L) L_{,r} dr, \tag{12}$$

where the determinant of the metric tensor is written as g. Figure 5 illustrates the radial change of the radiant energy flux over the disk for various values of α. It is apparent that the maximum flux is consistently higher in the case where $\alpha/M^2 = 2$ compared to Schwarzschild ($\alpha = 0$) and smaller values of α. The graph shows that smaller values of α not only diminish the maximum flux value but displace the peak to a smaller radial distance as well. It is worth noting that the locations where the flux reaches zero also shift toward smaller values of r. These points indicate the nearest section of the disk that is observable because of the radiation emitted by massive particles in those areas. These areas delineate the inner boundary of the accretion disk, aligning with the innermost stable circular orbits of test particles. Furthermore, our observations indicate that a smaller α results in the expansion of these orbits, as depicted in Figure 2.

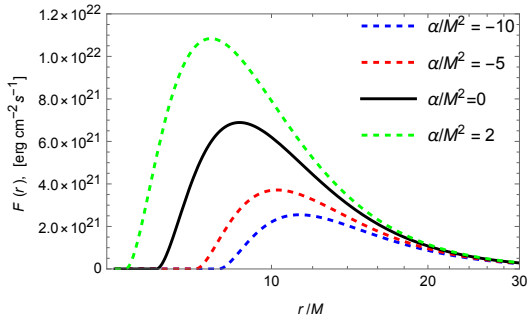

Figure 5. The radial distribution of the electromagnetic radiation flux emitted by the disk for various values of α.

The pivotal aspect of the mass accretion process is the efficiency with which the central object transforms incoming rest mass-accreting material into emitted electromagnetic radiation. This efficiency is primarily assessed by comparing two quantities measured at infinity: the rate of energy radiation from photons emitted by the disk's surface and successfully reaching infinity, and the rate of mass energy transportation to the central black hole. This comparison establishes the efficiency ratio. When all produced photons are able to freely escape to infinity, this efficiency can be characterized by the specific energy of massive particles at the innermost stable circular orbit

$$\eta = 1 - E_{ISCO}. \tag{13}$$

Using this relationship and Expression (8), we can derive η in tabular format, as illustrated in Table 1. It becomes apparent that the radiative efficiency escalates with higher values of α.

Table 1. Numerical data for variation of ISCO radius and η with change of α.

α/M^2	r_{ISCO}/M	$\eta\%$
-16	8.513	4.251
-10	7.907	4.580
-5	7.139	4.988
0	6.000	5.719
1	5.663	5.966
2	5.237	6.300

Numerical calculations reveal the relationship between the radiative efficiency of the disk and Gauss–Bonnet coupling constant α, which can be visualized in a plot as shown in Figure 6. The plot indicates that the lowest value of the radiative efficiency is approximately 4.2%. Moreover, as the parameter α increases, the efficiency rises steadily, reaching about 6.3% when $\alpha \to 2M^2$. Therefore, it can be concluded that the presence of a Gauss–Bonnet coupling constant does not affect the radiative efficiency of the disk considerably.

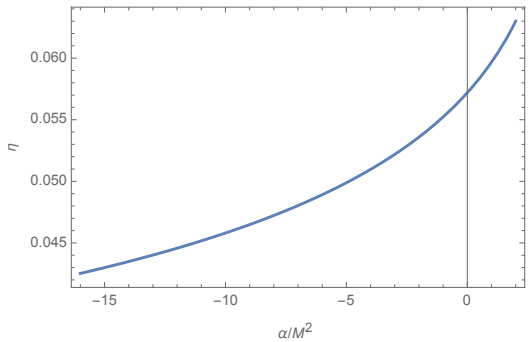

Figure 6. Continuous increase in radiation efficiency from disk as α increases.

In black body radiation, the flux, which can be expressed as $F = \sigma T^4$ where σ represents the Boltzmann constant, facilitates the demonstration of the radial variation of the disk temperature, as illustrated in Figure 7. It is clearly illustrated that an increase in α makes the temperature of the accretion disk higher in the close vicinity of the central black hole in 4D Einstein–Gauss– Bonnet gravity. By contrast, with respect to further distances, the effect of Gauss–Bonnet gravity does not differ noticeably from classical general relativity. The right panel of Figure 7 showcases the thermal profile of the disk given in energy units.

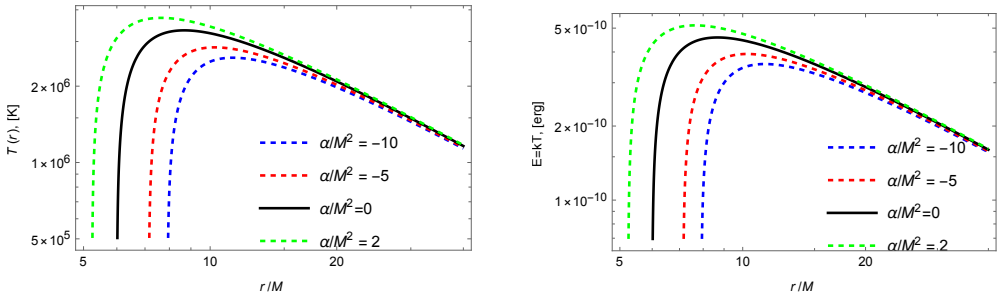

Figure 7. Temperature distribution across the disk for various values of the spacetime parameter α. On the left side, the temperature is expressed in Kelvin (K), and on the right, in energy units (erg).

To provide more comprehensive insight, illustrating the correlation between the temperature distribution and both the radius and GB parameter in a "density-plot" format would be advantageous, akin to the presentation in the left panel of Figure 8. In the plot, the purple region where the temperature is zero corresponds to the region inside the innermost stable circular orbits or inside the inner edge of the accretion disk around the black hole. The edge of this region clearly demonstrates the change of ISCO radius with the change of α. One can also see from the plot that the temperature of the accretion disk is higher where α is bigger and the distance from the black hole is smaller, as was discussed in the previous paragraph. An even clearer illustration of the radial change of the temperature of the accretion disk is given in the right plot of Figure 8 for the fixed value of α. The black circle in the center illustrates the black hole event horizon and the purple shaded region represents the inner part of the accretion disk. It can be observed that the temperature of the accretion disk starting from zero starts increasing very quickly near the inner edge of the accretion disk, reaches its biggest value; after that, it starts decreasing slowly when the distance from the central black hole increases.

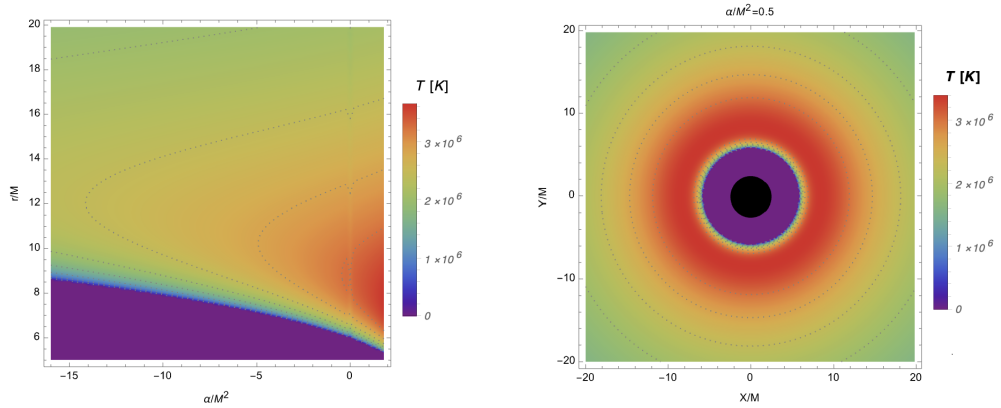

Figure 8. Temperature distribution in density-plot format. On right, X and Y represent Cartesian coordinates, while X-Y plane is situated on equatorial plane.

The dependence of the luminosity of the radiation from the frequency can be determined using the following [39]:

$$L(\nu) = 4\pi d_L^2 I(\nu) = \frac{8}{\pi} \cos i \int_{r_{in}}^{r_{ex}} \int_0^{2\pi} \frac{\nu_e r d\phi dr}{exp(\nu_e/T) - 1} . \tag{14}$$

Here, d_L represents the distance from the observer to the distant source, i is the inclination angle of the accretion disk, r_{in} refers to the inner radius of the disk, r_{ex} indicates the outermost radius of the disk, and $I(\nu)$ denotes the Planck distribution function. We can set $r_{in} = r_{ISCO}$ and $r_{ex} \to \infty$, considering that at infinity, as $r \to \infty$, the flux over the

disk's surface diminishes, as it does for any astronomical object. The emitted frequency $\nu_e = \nu(1+z)$ is determined by the redshift factor z, which is expressed as follows:

$$1+z = \frac{1+\Omega r \sin\phi \sin i}{\sqrt{-g_{tt} - 2\Omega g_{t\phi} - \Omega^2 g_{\phi\phi}}}, \tag{15}$$

where light bending is not taken into account [40,41]. Now, one can analyse the luminosity of radiation of the accretion disk. The dependence of the luminosity of electromagnetic radiation from the frequency of the radiation is given in Figure 9 for selected values of the Gauss–Bonnet coupling constant α. From the figure, one can notice that the maximum intensity of thermal radiation is around $\sim 1.5 \times 10^{17}$ Hz or ~ 0.6 keV, corresponding to electromagnetic radiation in the soft X-ray band. It is also apparent that the luminosity of the accretion disk of a static black hole in Gauss–Bonnet gravity is always lower than that of a black hole in general relativity. We see that in the case of a black hole in Gauss–Bonnet gravity, the luminosity of the accretion disk increases with the increase in α and the maximum point of lines shifts toward higher frequencies. It is also worth noting that for the smallest value of $\alpha = 10\ M^2$, the maximum value of the luminosity is smaller about three times as compared to the maximum possible value of $\alpha = 2\ M^2$ and about five times compared to Schwarzschild black hole.

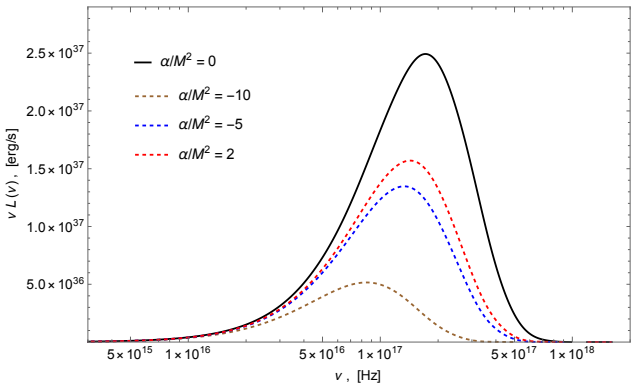

Figure 9. Spectral properties of the accretion disk surrounding a static black hole in EGB gravity. The inclination angle is set to be $i = \pi/6$. The graph is displayed on a standard scale near the region where the lines reach their maxima.

5. Summary

In this research, we focused on the characteristics of accretion disk around a static, spherically symmetric black hole in 4D Einstein–Gauss–Bonnet gravity, characterized by an additional coupling constant, α, in the spacetime metric. The well-known Novikov–Thorne accretion disk model was used to explore the thermal properties of the disk. We found the energy, angular momentum, and effective potential of a massive test particle moving in the accretion disk around the central black hole. Our results show that increasing α decreases all these quantities for a fixed radial distance from the black hole and shifts the corresponding radial profiles toward the central compact object. By comparing the ISCO radius in both the static black hole solution in Einstein–Gauss–Bonnet gravity and the Kerr black hole in general relativity, we found that the spin of the latter can be mimicked by α, up to $a \simeq 0.23M$, when α reaches its maximum value.

Our investigation of the thermal radiation flux from the accretion disk revealed that higher values of α increase the flux and shift its maximum closer to the black hole. At larger distances, the influence of the Gauss–Bonnet term diminishes, restoring the Schwarzschild black hole case. Calculations of the radiative efficiency showed that the effect of α is rela-

tively weak, causing only slight increases or decreases in efficiency as α varies. Assuming the thermal radiation behaves as black-body radiation, we found that the disk's temperature peaks slightly far from its inner edge and decreases with distance from the black hole, with higher values of α leading to higher temperatures.

Finally, we analyzed the electromagnetic spectra and discovered that the luminosity of the accretion disk in Einstein–Gauss–Bonnet gravity is consistently lower than that of a black hole in general relativity. We also found that increasing α shifts the peak luminosity toward higher electromagnetic frequencies, corresponding to the soft X-ray band.

Author Contributions: Investigation, O.K.; formal analysis, O.K.; writing—original draft, O.K., B.N. and B.A.; methodology, O.K., B.N. and B.A.; project administration, B.N. and B.A.; supervision, B.N. and B.A.; writing—review and editing, B.N. and B.A. All authors have read and agreed to the published version of the manuscript.

Funding: This research received no external funding.

Data Availability Statement: Data are contained within the article.

Conflicts of Interest: The authors declare no conflicts of interest.

References

1. Blázquez-Salcedo , J.L.; Macedo, C.F.B.; Cardoso, V.; Ferrari, V.; Gualtieri, L.; Khoo, F.S.; Kunz, J.; Pani, P. Perturbed black holes in Einstein-dilaton-Gauss-Bonnet gravity: Stability, ringdown, and gravitational-wave emission. *Phys. Rev. D* **2016**, *94*, 104024. [CrossRef]
2. Maselli, A.; Gualtieri, L.; Pani, P.; Stella, L.; Ferrari, V. Testing Gravity with Quasi Periodic Oscillations from accreting Black Holes: The Case of the Einstein-Dilaton-Gauss-Bonnet Theory. *Astrophys. J.* **2015**, *801*, 115. [CrossRef]
3. Ayzenberg, D.; Yagi, K.; Yunes, N. Linear Stability Analysis of Dynamical Quadratic Gravity. *Phys. Rev. D* **2014**, *89*, 044023. [CrossRef]
4. Konoplya, R.A.; Pappas, T.; Zhidenko, A. Einstein-scalar–Gauss-Bonnet black holes: Analytical approximation for the metric and applications to calculations of shadows. *Phys. Rev. D* **2020**, *101*, 044054. [CrossRef]
5. Nampalliwar, S.; Bambi, C.; Kokkotas, K.; Konoplya, R. Iron line spectroscopy with Einstein–dilaton–Gauss–Bonnet black holes. *Phys. Lett. B* **2018**, *781*, 626–632. [CrossRef]
6. Konoplya, R.A.; Stuchlík, Z.; Zhidenko, A. Axisymmetric black holes allowing for separation of variables in the Klein-Gordon and Hamilton-Jacobi equations. *Phys. Rev. D* **2018**, *97*, 084044. [CrossRef]
7. Kokkotas, K.D.; Konoplya, R.A.; Zhidenko, A. Analytical approximation for the Einstein-dilaton-Gauss-Bonnet black hole metric. *Phys. Rev. D* **2017**, *96*, 064004. [CrossRef]
8. Zinhailo, A.F. Quasinormal modes of Dirac field in the Einstein–Dilaton–Gauss–Bonnet and Einstein–Weyl gravities. *Eur. Phys. J. C* **2019**, *79*, 912. [CrossRef]
9. Cuyubamba Espinoza, M.A. Black Holes and Wormholes in Higher-Curvature Corrected Theories of Gravity. Ph.D. Thesis, ABC Federal University, Santo André, Brazil, 2019.
10. Younsi, Z.; Zhidenko, A.; Rezzolla, L.; Konoplya, R.; Mizuno, Y. New method for shadow calculations: Application to parametrized axisymmetric black holes. *Phys. Rev. D* **2016**, *94*, 084025. [CrossRef]
11. Glavan, D.; Lin, C. Einstein-Gauss-Bonnet Gravity in Four-Dimensional Spacetime. *Phys. Rev. Lett.* **2020**, *124*, 081301. [CrossRef]
12. Gürses, M.; Şişman, T.c.; Tekin, B. Is there a novel Einstein–Gauss–Bonnet theory in four dimensions? *Eur. Phys. J. C* **2020**, *80*, 647. [CrossRef]
13. Hennigar, R.A.; Kubizňák, D.; Mann, R.B.; Pollack, C. On taking the D $\to$ 4 limit of Gauss-Bonnet gravity: Theory and solutions. *JHEP* **2020**, *07*, 027. [CrossRef]
14. Bonifacio, J.; Hinterbichler, K.; Johnson, L.A. Amplitudes and 4D Gauss-Bonnet Theory. *Phys. Rev. D* **2020**, *102*, 024029. [CrossRef]
15. Arrechea, J.; Delhom, A.; Jiménez-Cano, A. Inconsistencies in four-dimensional Einstein-Gauss-Bonnet gravity. *Chin. Phys. C* **2021**, *45*, 013107. [CrossRef]
16. Aoki, K.; Gorji, M.A.; Mukohyama, S. A consistent theory of $D \to 4$ Einstein-Gauss-Bonnet gravity. *Phys. Lett. B* **2020**, *810*, 135843. [CrossRef]
17. Aoki, K.; Gorji, M.A.; Mukohyama, S. Cosmology and gravitational waves in consistent $D \to 4$ Einstein-Gauss-Bonnet gravity. *JCAP* **2020**, *9*, 014; Erratum in *JCAP* **2021**, *5*, E01. [CrossRef]

18. Hakimov, A.; Abdujabbarov, A.; Narzilloev, B. Quantum interference effects in conformal Weyl gravity. *Int. J. Mod. Phys. A* **2017**, *32*, 1750116. [CrossRef]
19. Narzilloev, B.; Ahmedov, B. Observational and Energetic Properties of Astrophysical and Galactic Black Holes. *Symmetry* **2023**, *15*, 293. [CrossRef]
20. Narzilloev, B.; Abdujabbarov, A.; Hakimov, A. Redshift of photons emitted from the accretion disk of a regular black hole surrounded by dark matter. *Int. J. Mod. Phys. A* **2022**, *37*, 2250144. [CrossRef]
21. Mirzaev, T.; Li, S.; Narzilloev, B.; Hussain, I.; Abdujabbarov, A.; Ahmedov, B. Simulated image of the shadow of the Kerr-Newman-NUT-Kiselev black hole in the Rastall gravity with a thin accretion disk. *Eur. Phys. J. Plus* **2023**, *138*, 47. [CrossRef]
22. Narzilloev, B.; Ahmedov, B. The eye of the storm: Optical properties. *Int. J. Mod. Phys. A* **2023**, *38*, 2350026. [CrossRef]
23. Abdulxamidov, F.; Benavides-Gallego, C.A.; Narzilloev, B.; Hussain, I.; Abdujabbarov, A.; Ahmedov, B.; Xu, H. Dynamics of spinning test particles around the Kerr-Newman-NUT black hole with quintessence in the Rastall gravity. *Eur. Phys. J. Plus* **2023**, *138*, 635. [CrossRef]
24. Alibekov, H.; Narzilloev, B.; Abdujabbarov, A.; Ahmedov, B. Frequency Shift of Photons in the Spacetime of Deformed RN BH. *Symmetry* **2023**, *15*, 1414. [CrossRef]
25. Alloqulov, M.; Narzilloev, B.; Hussain, I.; Abdujabbarov, A.; Ahmedov, B. Energetic processes around electromagnetically charged black hole in the Rastall gravity. *Chin. J. Phys.* **2023**, *85*, 302–317. [CrossRef]
26. Narzilloev, B.; Ahmedov, B. Thermal radiation of thin accretion disk around Taub-NUT black hole. *Int. J. Mod. Phys. D* **2023**, *32*, 2350064. [CrossRef]
27. Lovelock, D. The Einstein tensor and its generalizations. *J. Math. Phys.* **1971**, *12*, 498–501. [CrossRef]
28. Lovelock, D. The four-dimensionality of space and the einstein tensor. *J. Math. Phys.* **1972**, *13*, 874–876. [CrossRef]
29. Lanczos, C. A Remarkable property of the Riemann-Christoffel tensor in four dimensions. *Ann. Math.* **1938**, *39*, 842–850. [CrossRef]
30. Boulware, D.G.; Deser, S. String Generated Gravity Models. *Phys. Rev. Lett.* **1985**, *55*, 2656. [CrossRef]
31. Wheeler, J.T. Symmetric Solutions to the Maximally Gauss-Bonnet Extended Einstein Equations. *Nucl. Phys. B* **1986**, *273*, 732–748. [CrossRef]
32. Wiltshire, D.L. Spherically Symmetric Solutions of Einstein-maxwell Theory With a Gauss-Bonnet Term. *Phys. Lett. B* **1986**, *169*, 36–40. [CrossRef]
33. Cai, R.G. Gauss-Bonnet black holes in AdS spaces. *Phys. Rev. D* **2002**, *65*, 084014. [CrossRef]
34. Guo, M.; Li, P.C. Innermost stable circular orbit and shadow of the 4*D* Einstein–Gauss–Bonnet black hole. *Eur. Phys. J. C* **2020**, *80*, 588. [CrossRef]
35. Novikov, I.D.; Thorne, K.S. Astrophysics and black holes. In Proceedings of the Les Houches Summer School of Theoretical Physics: Black Holes, Les Houches, France, 1 August 1973; pp. 343–550.
36. Shakura, N.I.; Sunyaev, R.A. Black holes in binary systems. Observational appearance. *Astron. Astrophys.* **1973**, *24*, 337–355.
37. Page, D.N.; Thorne, K.S. Disk-Accretion onto a Black Hole. Time-Averaged Structure of Accretion Disk. *Astrophys. J.* **1974**, *191*, 499–506. [CrossRef]
38. Banerjee, I.; Chakraborty, S.; SenGupta, S. Decoding signatures of extra dimensions and estimating spin of quasars from the continuum spectrum. *Phys. Rev. D* **2019**, *100*, 044045. [CrossRef]
39. Torres, D.F. Accretion disc onto a static non-baryonic compact object. *Nucl. Phys. B* **2002**, *626*, 377–394. [CrossRef]
40. Luminet, J.P. Image of a spherical black hole with thin accretion disk. *Astron. Astrophys.* **1979**, *75*, 228–235.
41. Bhattacharyya, S.; Misra, R.; Thampan, A.V. General Relativistic Spectra of Accretion Disks around Rotating Neutron Stars. *Astrophys. J.* **2001**, *550*, 841–845. [CrossRef]